Biochimica et Biophysica Acta 1840 (2014) 1657–1669

Contents lists available at ScienceDirect

Biochimica et Biophysica Acta

journal homepage: www.elsevier.com/locate/bbagen

Type 1 ribotoxin-curcin conjugated biogenic gold nanoparticles for a multimodal therapeutic approach towards brain cancer

M. Sheikh Mohamed, Srivani Veeranarayanan, Aby Cheruvathoor Poulose, Yutaka Nagaoka, Hiroaki Minegishi, Yasuhiko Yoshida, Toru Maekawa, D. Sakthi Kumar *

Bio-Nano Electronics Research Centre, Graduate School of Interdisciplinary New Science, Toyo University, 2100, Kujirai, Kawagoe, Saitama 350-8585, Japan

ARTICLE INFO

Article history:
Received 23 May 2013
Received in revised form 31 October 2013
Accepted 16 December 2013
Available online 20 December 2013

Keywords:
Gold nanoparticle
Curcin
Glioma
Photo-thermal ablation
Dual targeting

ABSTRACT

Background: Gliomas have been termed recurrent cancers due to their highly aggressive nature. Their tendency to infiltrate and metastasize has posed significant roadblocks to in attaining fool proof treatment solutions. An initiative to curb such a scenario was successfully demonstrated in vitro, utilizing a multi-conceptual gold nanoparticle based photo-thermal and drug combination therapy.
Methods: Gold nanoparticles (Au NPs) were synthesized with a highly environmentally benign process. The Au NPs were PEGylated and conjugated with folate and transferrin antibody to achieve a dual targeted nano-formulation directed towards gliomas. Curcin, a type 1 ribosome inactivating protein, was attached to the Au NPs as the drug candidate, and its multifarious toxic aspects analyzed in vitro. NIR photo-thermal properties of the Au nano-conjugates were studied to selectively ablate the glioma cancer colonies.
Results: Highly cyto-compatible, 10–15 nm Au NP conjugates were synthesized with pronounced specificity towards gliomas. Curcin was successfully conjugated to the Au NPs with pH responsive drug release. Prominent toxic aspects of curcin, such as ROS generation, mitochondrial and cytoskeletal destabilization were witnessed. Excellent photo-thermal ablation properties of gold nanoparticles were utilized to completely disrupt the cancer colonies with significant precision.
Conclusion: The multifunctional nanoconjugate projects its competence in imparting complete arrest of the future proliferation or migration of the cancer mass.
General significance: With multifunctionality the essence of nanomedicine in recent years, the present nanoconjugate highlights itself as a viable option for a multimodal treatment option for brain cancers and the like.

1. Introduction

Treatments of cancers related to the brain have posed extreme complications due to their location and the complexity in reaching them. The most common and chronic type of brain cancers are the gliomas [1–3]. These originate from glial cells and are highly vascularized. They possess the tendency to aggressively infiltrate and are associated with cases of extensive necrosis and hypoxia in addition to severe disruption of the blood brain barrier (BBB), thereby compromising the integrity of the brain. Gliomas are commonly referred to as recurrent cancers, as they intrusively grow back, even after comprehensive surgical excisions [4,5]. Also, the surgical procedures often add to the risk of metastasis, increasing the chances of possible future malignancies at multiple locations. Chemotherapeutics rarely reach these tumors, mainly due to the selective trafficking monitored by the BBB, and are also accompanied by the non-specific targeting and accumulation risk to normal cells [6]. Other options such as radiotherapy, accompany imminent short and long-term side effects as normal cells and organs are unintentionally exposed to the radiation [7]. Cumulatively, gliomas have been considered as rarely curable and the demand for alternative promising solutions has taken the forefront.

The nanomedicine platform offers exciting options for treatment of numerous life consuming ailments [8–11]. The focal core of this technology employing diverse nano-vehicles, lies in the claim to achieve maximum specificity with minimal side effects by the incorporation of single or multiple targeting ligands [12,13]. The meager quantity of drug requirements compared to conventional chemotherapy approaches, with the possibility of monitoring their fate by the conjugation of various imaging agents, proves a highly supportive factor. The majority of tumors express fenestrated neo-vasculature along with inferior lymphatic drainage, which presents the nano-drug delivery systems (NDDS) to preferentially accumulate at the tumor site over time [14]. Owing to their intriguing features as size, shape, high biocompatibility, etc., gold nanoparticles (Au NPs) have been receiving increased attention in the area of NDDS, as a variety of drugs, proteins, antibodies, peptides, etc., can be conjugated with them [15–17]. Apart from their ease of synthesis, control over shape/size and the relative

* Corresponding author. Tel.: +81 492 39 1636; fax: +81 492 34 2502.
E-mail address: sakthi@toyo.jp (D.S. Kumar).

0304-4165/$ – see front matter © 2013 Elsevier B.V. All rights reserved.
http://dx.doi.org/10.1016/j.bbagen.2013.12.020

facile modes of surface modifications, Au NPs have been widely acclaimed for their thermal characteristics, which could be efficiently harnessed for photo-thermal ablation applications [18–22].

In this study, we present a multifunctional, PEGylated, biogenic Au NP based nanocarrier, capable of delivering a potent ribosome inactivating protein (RIP), curcin, which has been previously attributed with protein synthesis inhibition [23,24], cellular organelle disruption, cytoskeletal damage, etc., (unpublished) specifically targeting glioma cells. A dual targeted approach was successfully attempted employing folate and anti-transferrin antibody, to achieve maximum specificity towards glioma. Curcin was conjugated with the Au NPs via pH-sensitive bonds to effectuate pH-controlled release in the acidic environments of tumor cells, thereby rendering it benign to normal cells. Curcin exhibited superior therapeutic efficacy by curbing the migratory and proliferative properties of glioma cells in mono-layered as well as in 3D glioma spheroids. The 3D spheroids mimic, to an extent, the in vivo scenario, where the cancer cells proliferate as a solid mass, therefore the effects of curcin on such an in vitro mass may, in principle, be advantageous to suppress the propagation of in vivo tumor masses as well. The Au NPs, apart from their role as efficient drug carriers, were tested for their excellent thermal properties under NIR influence, to ablate the cancer cells and 3D cancer colonies in a controlled fashion. It is proposed

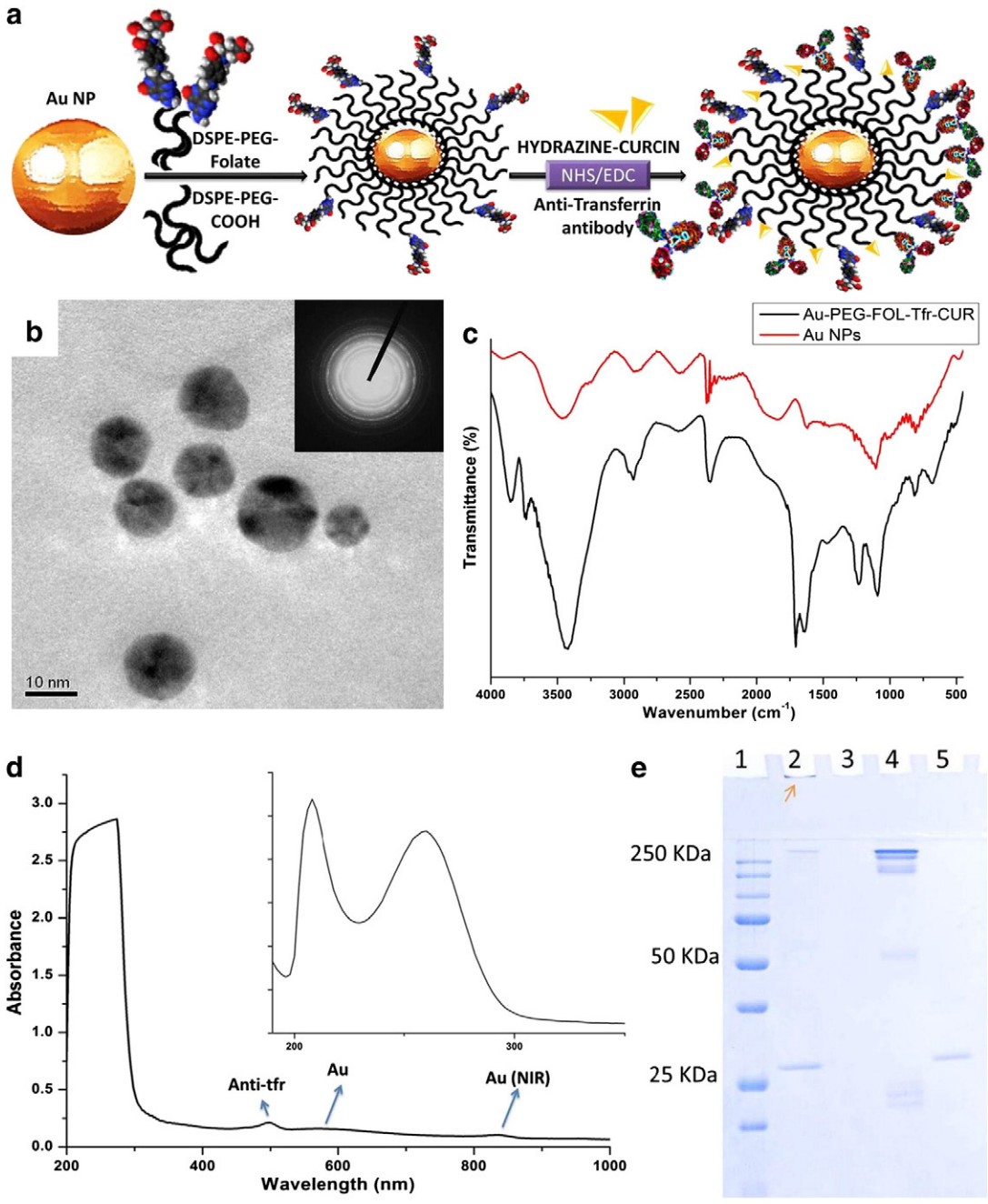

Fig. 1. (a) Preparation scheme of Au-PEG FOL-Tfr-CUR conjugate. (b) HRTEM image of bio-functionalized Au NPs (inset: SAED pattern). (c) FT-IR spectrum of Au NPs synthesized as such and after bio-functionalization. (d) UV–vis spectra of Au-PEG FOL-Tfr-CUR conjugate exhibiting the absorption of curcin at 220 and 272 nm (inset), the absorption of transferrin centered at 490 nm, broad SPR of Au NPs centered at 520 nm and NIR absorption of Au NPs around 800 nm. (e) CBB stained SDS PAGE of Au-PEG FOL-CUR-Tfr conjugate. Lane 1: protein marker, Lane 2: Au-PEG FOL-CUR-Tfr, Lane 3: filtrate post 50 KDa ultra-centrifugal filtration, Lane 4: anti-transferrin antibody and Lane 5: curcin (28.2 KDa). The conjugation of Tfr antibody and curcin to the Au NPs is confirmed by the presence of corresponding bands. The arrow indicates the Au NPs which failed to electrophorese and settled in the loading wells itself.

that the tumor-targeted chemotherapy, combined with the exceptional photo-thermal ablation ability of Au NPs can significantly enhance the therapeutic options against human gliomas.

2. Materials

Dulbecco's modified eagle's medium (DMEM), 0.25% Trypsin, phosphate buffered saline (PBS) (pH 7.2), Fetal bovine serum (FBS), antibiotics (Penicillin, Streptomycin), chloroauric acid ($HAuCl_4.3H_2O$), Reactive oxygen species (ROS) variety pack, actin phalloidin rhodamine, Calcein/Propidium iodide (PPI) stain, and monoclonal anti-vinculin antibody were purchased from Sigma-Aldrich. Alamar Blue, Image-iT™ LIVE Mitochondrial Transition Pore Assay Kit, mouse monoclonal anti-transferrin antibody were from Invitrogen. Geltrex was acquired from Gibco. Secondary antibodies to transferrin (Tfr) and Anti-Histone H2A.X antibody were procured from abcam. DSPE-PEG-COOH {1,2-distearoyl-*sn*-glycero-3-phosphoethanolamine-N-[carboxy(polyethylene glycol)-2000] (ammonium salt)}, DSPE-PEG-FOL {1,2-distearoyl-*sn*-glycero-3-phosphoethanolamine-N-[folate(polyethylene glycol)-2000] (ammonium salt)} and PEG2000 PE CF {1,2-distearoyl-*sn*-glycero-3-phosphoethanolamine-N-[poly(ethylene glycol)2000-N′-carboxyfluorescein] (ammonium salt)} were purchased from Avanti polar lipids. All other chemicals and reagents were of analytical grade acquired from either Sigma-Aldrich or Wako chemicals.

2.1. Preparation and biofunctionalization of Au NPs

Water-dispersible Au NPs were prepared according to our previous report [25] with minor modifications. Briefly, a solution of 1 $mmolL^{-1}$ $HAuCl_4.3H_2O$ was prepared in Milli Q water. 5 ml of this solution was mixed with an equal volume of aqueous extract of *Jatropha curcas* seed shells and incubated overnight in a heated shaking water bath (90 ºC). The nanoparticles thus obtained were centrifuged and thoroughly washed with Milli Q water and stored at room temperature until further use. A solution of 1 mg/ml of the Au NPs in chloroform was prepared. To this suspension, 200 μl of DSPE-PEG-COOH (0.2 M), DSPE-PEG-FOL (0.02 M) and PEG2000 PE CF (0.02 M) were added and the solution was gently evaporated to obtain a thin film of Au NPs and PEG-lipid. This thin film was then hydrated with 70 ºC PBS buffer and the suspension was stirred vigorously under heat to obtain a clear aqueous suspension of Au NPs functionalized with PEG moieties (Au-PEG COOH-FOL). The Au-PEG COOH-FOL NPs (without PEG2000 PE CF) were conjugated to transferrin antibodies by EDC-NHS activation, utilizing the free COOH units on Au NPs surface to synthesize dual targeted nano-conjugates (Au-PEG FOL-Tfr), devoid of drug. This reaction produces a stable amide bond between primary amines on the antibody and carboxyl groups on the PEG chain that is exposed. Meanwhile, another set of the EDC-NHS activated PEG functionalized Au NPs were allowed to react with anti-Tfr antibody and hydrazine monohydrate pre-treated curcin solution (100 μg/ml) overnight at 4 ºC to obtain dual targeted, drug loaded version. After the incubation, the solution was centrifuged using 50 KDa (Amicon Ultra, Millipore) centrifugal filter units to obtain the retentate, consisting of the drug conjugated, PEG functionalized Au NPs (Au-PEG FOL-Tfr-CUR). The synthesis procedure has been represented in Fig. 1a.

2.2. Cell culture maintenance

Glioma (human brain glioblastoma) and HCN-1A (human cortical neurons) cell lines were acquired from Riken Bioresources, Japan and ATCC respectively, and maintained in T25 flasks using DMEM medium supplemented with 10% FBS and antibiotics in an incubator at 37 °C with 5% CO_2. The cells were sub-cultured every 2 days. Cells were cultured on glass base dishes for confocal microscopy studies and in 96 well plates for cytotoxicity studies. For 3D cancer assay, approximately 25,000 glioma cells were seeded onto 100 μl Geltrex coated wells and were cultured for 4 days to allow the formation of 3D spheroids.

2.3. Particle characterization studies

The morphology of as prepared Au-PEG FOL-Tfr-CUR was analyzed with the help of field emission transmission electron microscope (TEM), (JEOL JEM-2200-FS) and average size determined by Nano-ZS Zetasizer (Malvern Instruments Ltd). Fourier transform infrared spectroscopy (Spectrum 100 FT-IR Spectrometer, Perkin Elmer) analysis was performed to investigate the surface chemical bonding and characteristics of bare Au NPs and Au-PEG FOL-Tfr-CUR NPs. UV–vis spectrophotometry (Shimadzu UV-2100PC/3100PC UV visible spectrometer) and SDS PAGE were carried out to analyze the drug/antibody attachment onto Au NPs.

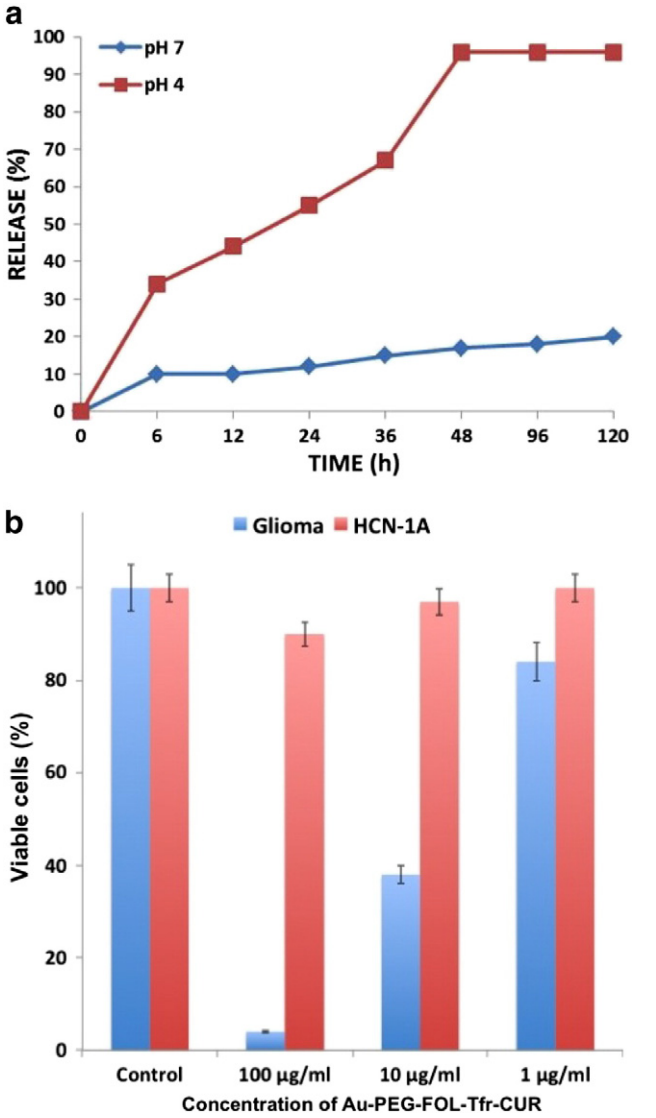

Fig. 2. (a) pH dependent curcin release from Au-PEG FOL-Tfr-CUR conjugate. The release of curcin at pH 4 was found to be gradual and nearly 100% release was observed by 2 days. The drug release at physiological pH 7 was found to be slow and controlled till the observed period of 5 days with a maximum release recorded to be around 20% by day 5. (b) Cytotoxicity analysis of the Au NP conjugates. The Au-PEG FOL-Tfr-CUR conjugates at the concentration of 100 μg/ml rendered selective toxicity to glioma cells, killing 97% of them by day 2 whereas the normal neuronal cells remained 90% viable. The slight compromise in the viability of HCN-1A might be due to the detachment of minute quantities of poorly adhered curcin onto the Au NPs. The observations confirm the high specificity of dual targeted NPs and also the tuned lethal effect of curcin towards cancer cells alone.

The amount of curcin conjugated onto the NPs was evaluated by utilizing the following formula:

$$\text{Curcin conjugation } (\%) = \frac{\text{Absorbance of conjugated curcin}}{\text{Absorbance of curcin used}} \times 100.$$

The standard absorption of the drug, curcin at various concentrations was plotted and the drug release profile at varied time intervals was analyzed using the standard curve of the drug's absorbance. pH 7, depicting the physiological pH and pH 4, depicting the acidic pH of cancer cells were utilized for drug release studies. 1 ml of freshly prepared Au-PEG FOL-Tfr-CUR NPs in respective pH solutions were

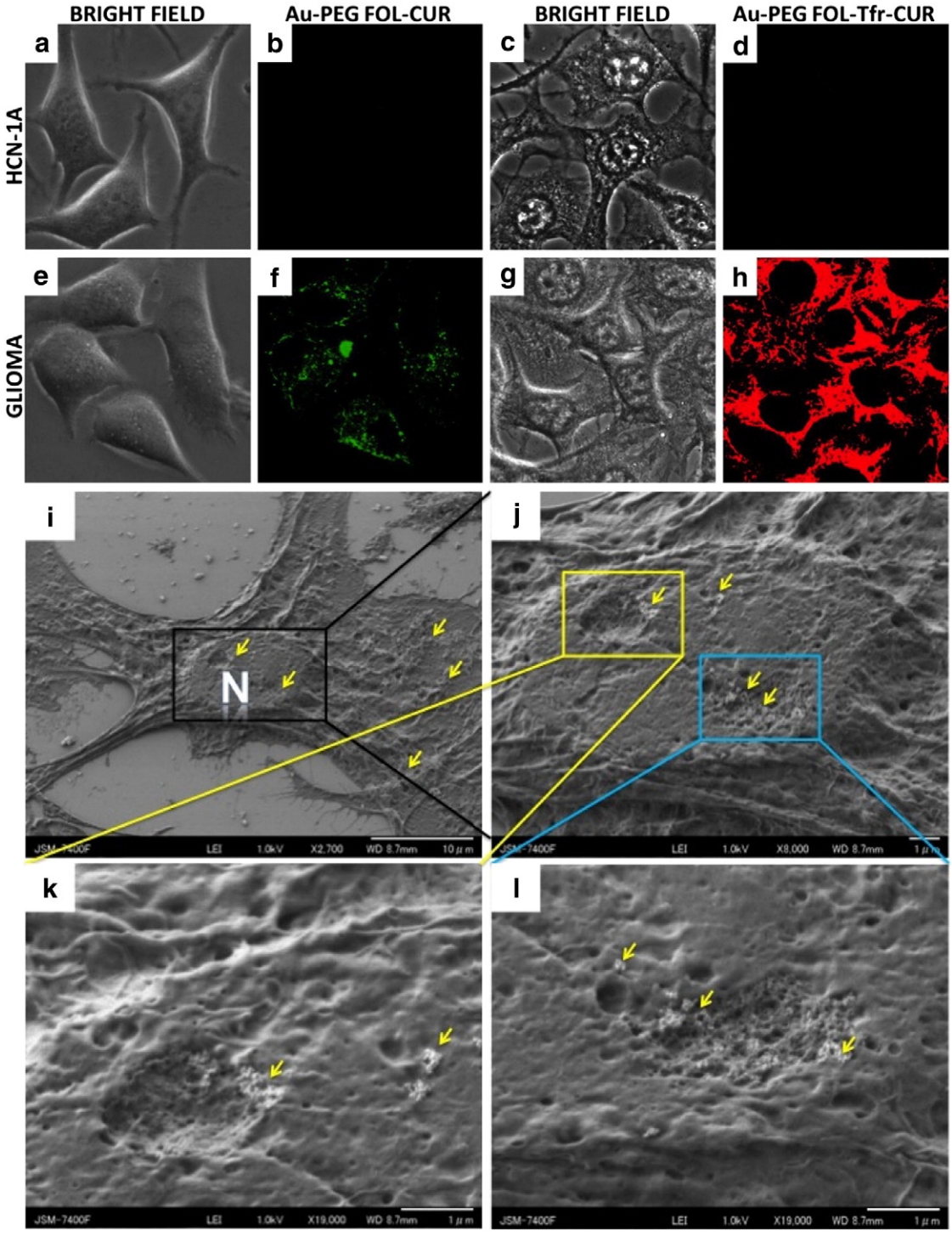

Fig. 3. Cellular uptake of single, Au-PEG FOL and dual targeted Au-PEG FOL-Tfr NPs. The Au-PEG FOL and Au-PEG FOL-Tfr NPs gained selective entry into glioma cells (f and h) sparing normal HCN-1A (b and d). The corresponding bright field images of normal (a and c) and cancer cells (e and g) are shown. The enhanced intensity from the gliomas treated with Au-PEG FOL-Tfr provide proof of the successful conjugation of dual targeting ligands to the Au NPs, in addition to the increased particle uptake which can be directly correlated to the observed fluorescence. FESEM images (i–l) provide evidence of the adherence of nanoparticles throughout the cellular body gaining entry at multiple locations including the nuclear regions (arrows) facilitated by the formation of endocytic burrows (k and l).

analyzed at different points of time using UV–vis absorption spectroscopy.

2.4. Cell culture techniques

Cytotoxicity was assayed with the help of alamar blue. In principle, only metabolically active cells can convert the non-fluorescent alamar blue into a fluorescent moiety, whose absorbance could be read at 560 nm. Cells, glioma and HCN-1A were trypsinized and pelleted. 5000 cells were counted and added to wells of 96 well plates and grown for 24 h prior to NP exposure. All experiments were conducted in triplicates. Controls were maintained devoid of any treatment, whereas test groups were treated with 100 μl (1 μg/ml, 10 μg/ml and 100 μg/ml) of drug loaded dual targeted Au NPs. The plates were incubated for 48 h after which the fluorescence intensity of the final product was analyzed with a microplate spectroflurimeter (Multidetection microplate scanner, Dainippon Sumitomo Pharma). The viable percentage of cells were calculated for each group and plotted against concentration of NPs. For analysis of targeting ability and induction of ROS, approximately 25,000 cells were plated onto 35 mm glass base dishes for 24 h. 100 μl of 100 μg/ml NPs were added to the plates, as this concentration was found to be the most lethal dose for gliomas, and incubated for 2 h at culture conditions. After the incubation period, cells were washed, fixed using acetone and treated with secondary antibody specific to anti-Tfr antibody. After 1 h, the cells were washed thoroughly and analyzed under an excitation wavelength of 561 nm under a high-speed confocal laser-scanning microscope (CLSM, Olympus IX 81 under DU897 mode) to visualize particle uptake. For scanning electron microscopy (JEOL, JSM-7400F, field emission SEM), cells were grown on cover slips for 24 h prior to nanoparticle exposure for 2 h, after which, the cells were washed and fixed using 4% glutaraldehyde. Fixed coverslips were sequentially dehydrated using increasing ethanol concentration and critical point dried before mounting onto SEM grid and analyzed. For ROS estimation, cells were treated with Au-PEG FOL-Tfr and Au-PEG FOL-Tfr-CUR NPs for 24 h, after which the cells were treated with ROS tracer dye. After 30 min of incubation, the cells were washed and viewed at 488 nm excitation under a CLSM. For mitochondrial pore transition assay, approximately 25,000 cells were seeded onto 35 mm glass base dishes. A test group of cells was treated with 100 μg/ml of Au-PEG FOL-Tfr-CUR NPs. After 48 h, the plates were stained for pore transition as per the manufacturer's instructions and analyzed under a CLSM. DNA fragmentation analysis was performed by treating the cells with 100 μg/ml of Au-PEG FOL-Tfr-CUR NPs for 48 h and fixing them prior to addition of anti-histone H2A.X antibody. Cells were washed in PBS and exposed to red fluorescent secondary antibodies to H2A.X for 1 h after which the cells were counterstained with Hoechst and observed for DNA fragmentation under 405 and 561 nm filters using CLSM. For vinculin analysis, cells were treated with 100 μg/ml concentration of Au-PEG FOL-Tfr-CUR NPs for 24 h. After the incubation period, cells were washed and fixed using formaldehyde and acetone and treated with antibodies to vinculin. After 1 h, the FITC conjugated secondary fluorescent antibodies (anti-antibody of primary antibody) were added and the plates were incubated for 1 h. Plates were then washed and observed under CLSM. Actin cytoskeletol staining was performed with phalloidin rhodamine post 24 h of Au-PEG FOL-Tfr-CUR NP treatment. Cells were visualized at an excitation wavelength 561 nm.

For photothermal ablation studies, approximately 25,000 cells were grown in glass base dishes. A highly monochromatic, collimated beam of NIR range (800 nm) [Chameleon Ultra diode-Pumped Mode Locked-

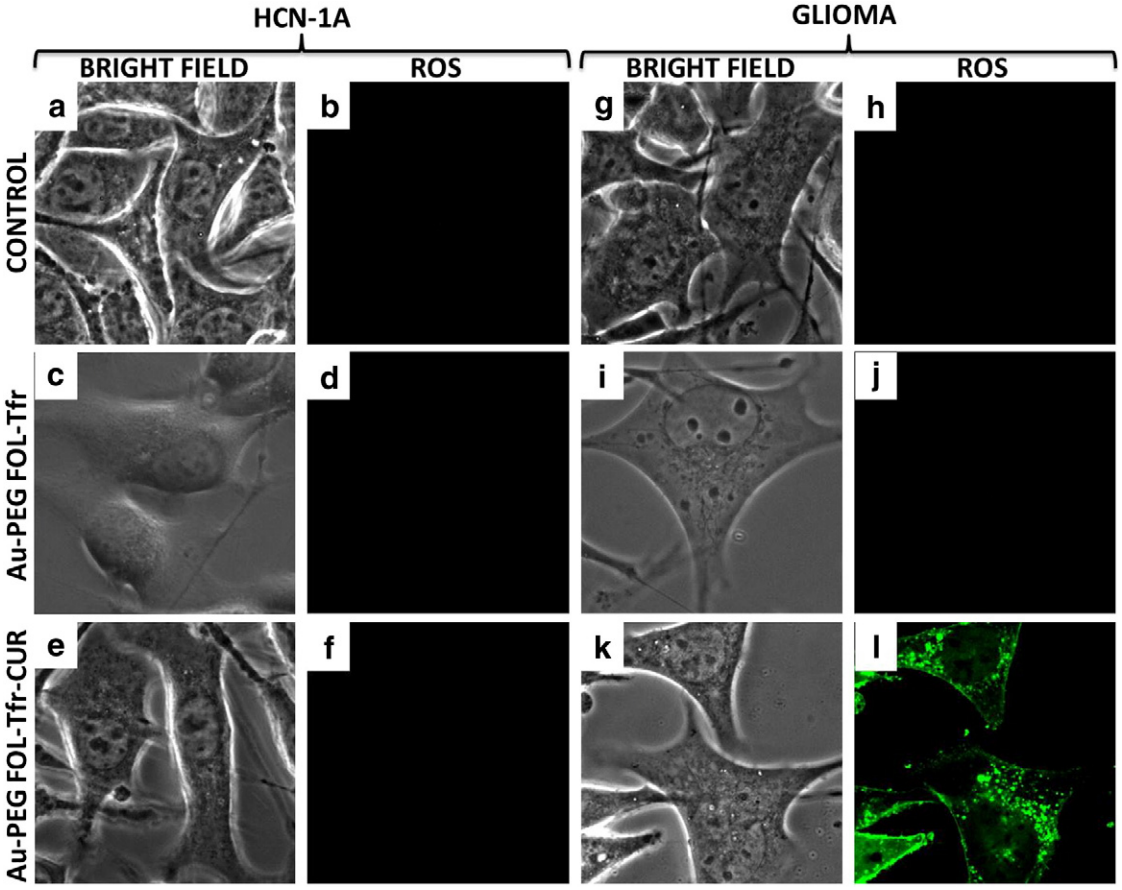

Fig. 4. Analysis of ROS generation in response to Au-PEG FOL-Tfr and Au-PEG FOL-Tfr-CUR. The nanoformulation devoid of curcin failed to generate ROS in both normal and glioma cells (d and j). On the contrary, the drug loaded NP conjugate generated significant ROS in cancer cells (l) whereas normal cells showed any ROS fluorescence (f).

Sub 200 Femtosecond Laser (Coherent 80 MHz repetition rate)] with power 1.726 W/cm^2 (Laser power meter: VEGA, OPHIR, Japan) was utilized. The temperature variations were measured with an infra-red (IR) thermometer [Thermal imager test 881-2 (Testo AG, Germany)]. The cells were treated with Au-PEG FOL-Tfr and Au-PEG FOL-Tfr-CUR NPs and subjected to NIR laser exposure for 5 s, after which they were stained using Calcein/PPI. Similarly, the test 3D spheroids were incubated with 100 μl of 100 μg/ml Au-PEG FOL-Tfr-CUR NPs for 48 h to study the effect of curcin and 2 h prior to photothermal ablation. After both the experiments, cells were stained with Calcein/PPI to analyze the live/dead populations. All the experiments were conducted in triplicates and the cells were thoroughly washed to remove unbound NPs and stains prior to analysis.

3. Results and discussion

To prepare the relatively monodisperse and highly cyto-compatible Au NPs, an environmentally conservative approach was adopted employing *J. curcas* seed shell extracts [25]. The synthesis process differs significantly from the conventional modes of bio-mediated NP synthesis, where the reducing sources (plant, micro-organisms) are used up and discarded, whereas in the present case the seed shells retain their inherent characteristics (minimal loss of ash content) which is their ability to serve as high value thermal energy sources. Therefore such an environmentally conservative approach could not only yield a variety of desired nanomaterials but also preserve the native properties of the reducing agents, contributing to the sustained utilization of bioresources. The Au NPs were in the size range of 5–10 nm (TEM observation) with an average size of 17.54 nm (PDI 0.164) according to zeta sizer. The bio-functionalization of bare Au NPs did not have any significant effects on their morphology as majority of the particles were in the range of 10–15 nm (Fig. 1b) according to TEM with a zeta sizer average of 22.66 nm (PDI 0.278) and were perfectly crystalline (Fig. 1b inset). The FT-IR spectrum of unmodified Au NPs and Au-PEG FOL-Tfr-CUR NPs is presented in Fig. 1c. The C–O–C ether stretch bands around 1175 cm^{-1} and 1099 cm^{-1} appear in the case of bio-functionalized Au NPs, which is absent in the bare NPs. Similarly, the band at 2918 cm^{-1} corresponds to CH_2 stretching vibrations. The characteristic IR absorption peak of folate at 1629 cm^{-1} was observed in the spectrum of bio-functionalized Au NPs. These signature peaks confirmed the successful functionalization of Au NPs with lipid-PEG conjugates [26,27]. The attachment of anti-Tfr and curcin onto PEG

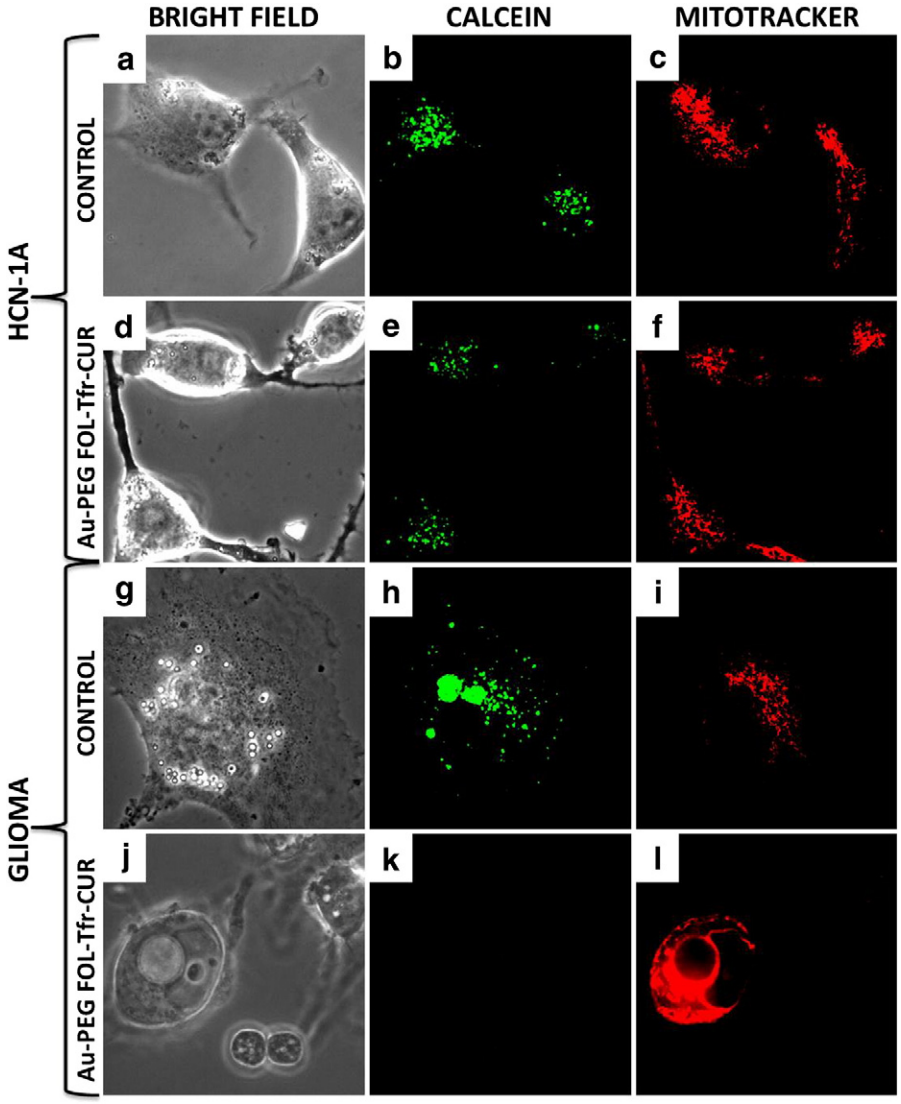

Fig. 5. Mitochondrial membrane potential destabilization. Discrete calcein signaling, indicative of properly functioning mitochondrial apparatus was clearly visualized in the case of controls (b, h) and Au-PEG FOL-Tfr-CUR treated HCN-1A (e). The complete lack of any such fluorescence signals from the Au-PEG FOL-Tfr-CUR treated glioma (k) suggested the absence of any functional mitochondria. Also, the bleached mitotracker staining (l) was indicative of formation of pores compromising mitochondrial membrane integrity which may have been due to the effects of curcin augmented generation of ROS leading to loss of membrane potential.

functionalized Au NPs was confirmed by the presence of N–H vibration at 3400–3200 cm^{-1}, C═O stretching at 1667 cm^{-1} and hydrazone C═N, N – N bands at 1470 cm^{-1} and 840 cm^{-1} respectively. Additionally, the conjugation of antibody to the Au NPs was affirmed by UV–vis spectroscopy (Fig. 1d). The absorbance peak at 490 nm relates to the presence of Tfr antibody [28]. SDS PAGE gel electrophoresis (Fig. 1e) was performed to re-affirm the presence of antibody in the nanoconjugate. The coomassie stained gel revealed the presence of anti-Tfr antibody (Fig. 1e, Lane 2) with signature bands corresponding to the standard (Lane 4). The Au NPs failed to electrophorese in the gel and remained stacked in the loading wells (Lane 2, arrow).

The drug loading and release from NPs were analyzed using UV–vis spectroscopy. The drug, curcin shows strong absorbance centered at 220 and 272 nm. The Au-PEG FOL-Tfr-CUR NPs exhibited a strong narrow peak in these signature absorbance regions, corresponding to curcin (Fig. 1d inset), along with the surface plasmon peak of Au at 521 nm [29]. The amount of conjugated drug was calculated by using this (curcin) absorption value and was determined to be 92%. Highly insignificant quantity of drug release from the particles suspended in pH 7, over a period of 5 days was recorded (Fig. 2a). An initial release of 10% of curcin occurred within 6 h after which an equal amount of release was witnessed over a period of 120 h. The initial 10% release could be attributed to the loosely adhered drugs onto the Au NPs. Whereas in the case of Au NPs suspended in pH 4 buffer, a gradual release of curcin was witnessed. Nearly 34% release within 6 h, followed by a slow and steady release was observed. 67% of the drug was released by 36 h, whereas 96% release occurred by 48 h which plateaued thereafter. These observations evidence the highly efficient pH dependent drug release achieved as a result of the hydrazine bonding [30,31]. Minimal drug release at pH 7 over 5 days confirmed that this formulation is safe and dependable against premature leakage of drugs at normal physiological pH. The extremely high levels of drug conjugation, aptly complemented by the pH controlled drug release, makes this nanoscheme a promising option for future NDDSs.

3.1. Cytotoxicity analysis

The cyto-compatibility of the bare Au NPs as such has been analyzed and reported previously [25]. The PEG functionalization of these NPs furthers their cyto-amiability. The Au-PEG FOL-Tfr-CUR NPs, at the highest concentration, 100 μg/ml, proved extremely detrimental to glioma cells with approximately 97% of the cells dead by 48 h (Fig. 2b). The results also depicted a dose dependent toxicity rendered by the drug with the cellular viability increasing with decrease in NP

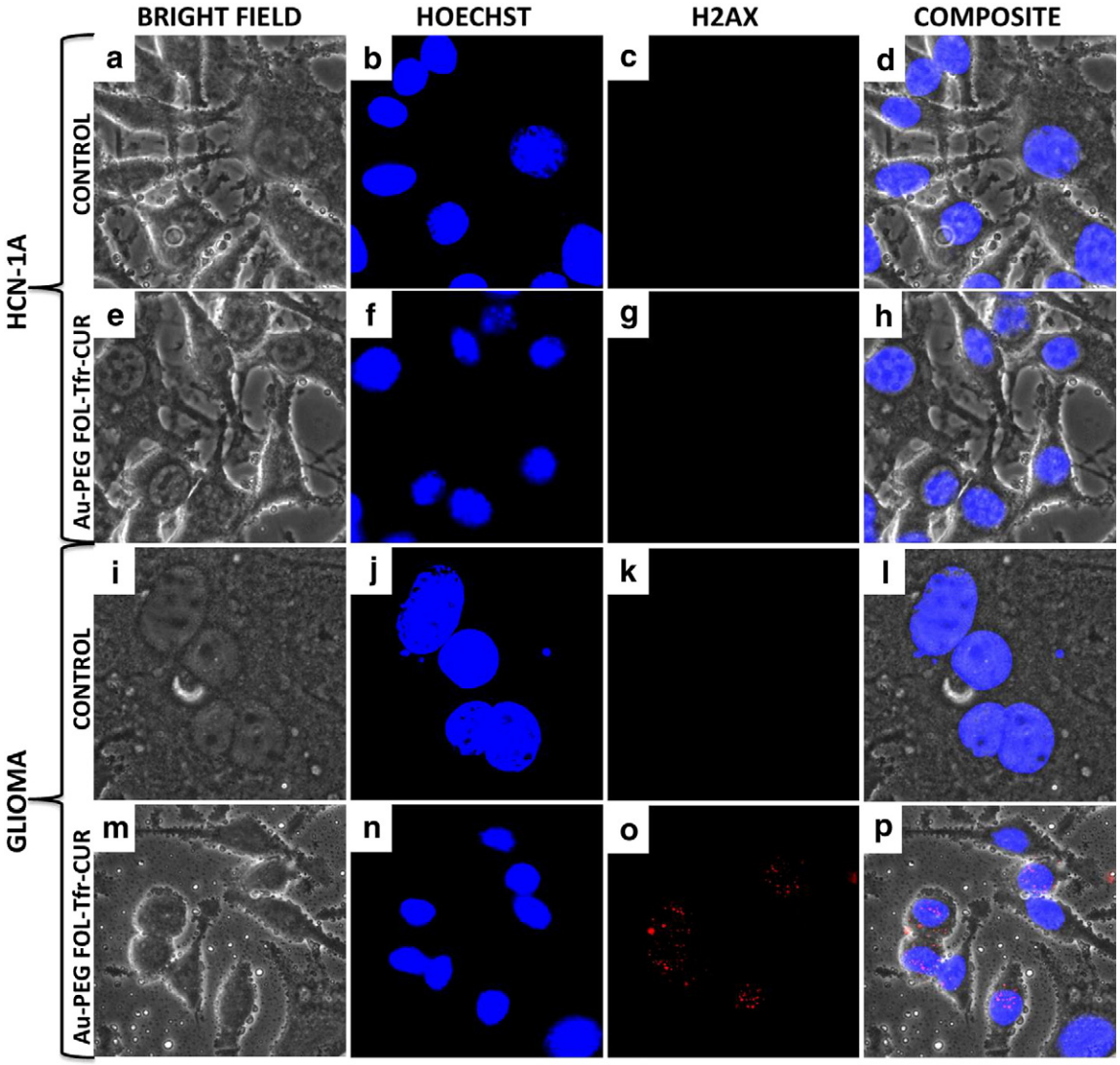

Fig. 6. Histone phosphorylation at DNA double-strand breaks. Nuclear toxicity to glioma was evident from the presence of double strand DNA breaks confined to nuclear region (o, discrete red fluorescence) which was absent in the case of test (g) and control groups (c, k). Such nuclear toxicity due to an exogenous toxin as curcin, could lead to detrimental effects and recruit apoptotic inducers leading to shutting down of the nuclear components and subsequent cell death.

concentration. Normal HCN-1A cells, at highest concentration of Au-PEG FOL-Tfr-CUR NPs showed slightly reduced viability (90%). The viability improved with decrease in NP concentration. The results were emulative of the drug release and NP cellular entry observations. The slight compromise in viability of the HCN-1A could be due to the early release of poorly adhered drug molecules from the Au NPs. Further increase in viability of HCN-1A, supports the successful attainment of high specificity and pH oriented release of drug. The feeble viability of gliomas is a concrete proof of the above claim. Thus, the observation with the toxicity data reasserts the theory of multi-target and controlled drug release achieved herein.

3.2. Cellular entry of NPs

The cellular uptake of Au-PEG FOL and Au-PEG FOL-Tfr NPs was adjudged by the fluorescence of FITC and the secondary antibodies, respectively, and visualized under CLSM (Fig. 3b, f & d, h). No visible signals were recorded from the normal, HCN-1A cells with both the single (Fig. 3b) and dual targeted (Fig. 3d) NPs. In the case of gliomas, the fluorescence with Au-PEG FOL (Fig. 3f) was comparatively reduced to the Au-PEG FOL-Tfr NPs (Fig. 3h). The presence of dual targeting moieties, both of which are overexpressed in gliomas, facilitated such a difference in the fluorescent intensities of single and dual targeted versions. Therefore it is safe to surmise that the overexpressed receptors for folate and transferrin on the glioma cells presented an enticing invitation to the nano-conjugates which was not the case with HCN-1A cells that lack these receptors in highly significant quantities, thereby arresting the NPs' entry into the normal and enhancing their entry into the cancer cells. The particle entry was also visualized with SEM (Fig. 3i–l) which revealed that a high concentration of nanoparticles was attached onto the cells with many in the process of endocytosis at multifarious locations spanning the entire spectrum of the cellular body. The multi-target approach is fast gaining pace in the nanomedicine arena, as it provides improved and efficient targeting of desired cells, especially cancer cells, to deliver the payloads of drugs or the like [32]. The results garnered in the present report not only supplement, but also encourage the utilization of multiple targeting schemes to achieve eminent specificity.

3.3. Multi-organelle therapeutic effects of Au-PEG FOL-Tfr-CUR NPs

Curcin is known to induce ROS, which affects mitochondrial permeability and leads to programmed cell death (unpublished). Glioma cells showed discrete signals of ROS in the cytoplasm (Fig. 4l), which was absent with HCN-1A (Fig. 4f) on treatment with Au-PEG FOL-Tfr-CUR NPs. Also, the absence of any signals from the Au-PEG

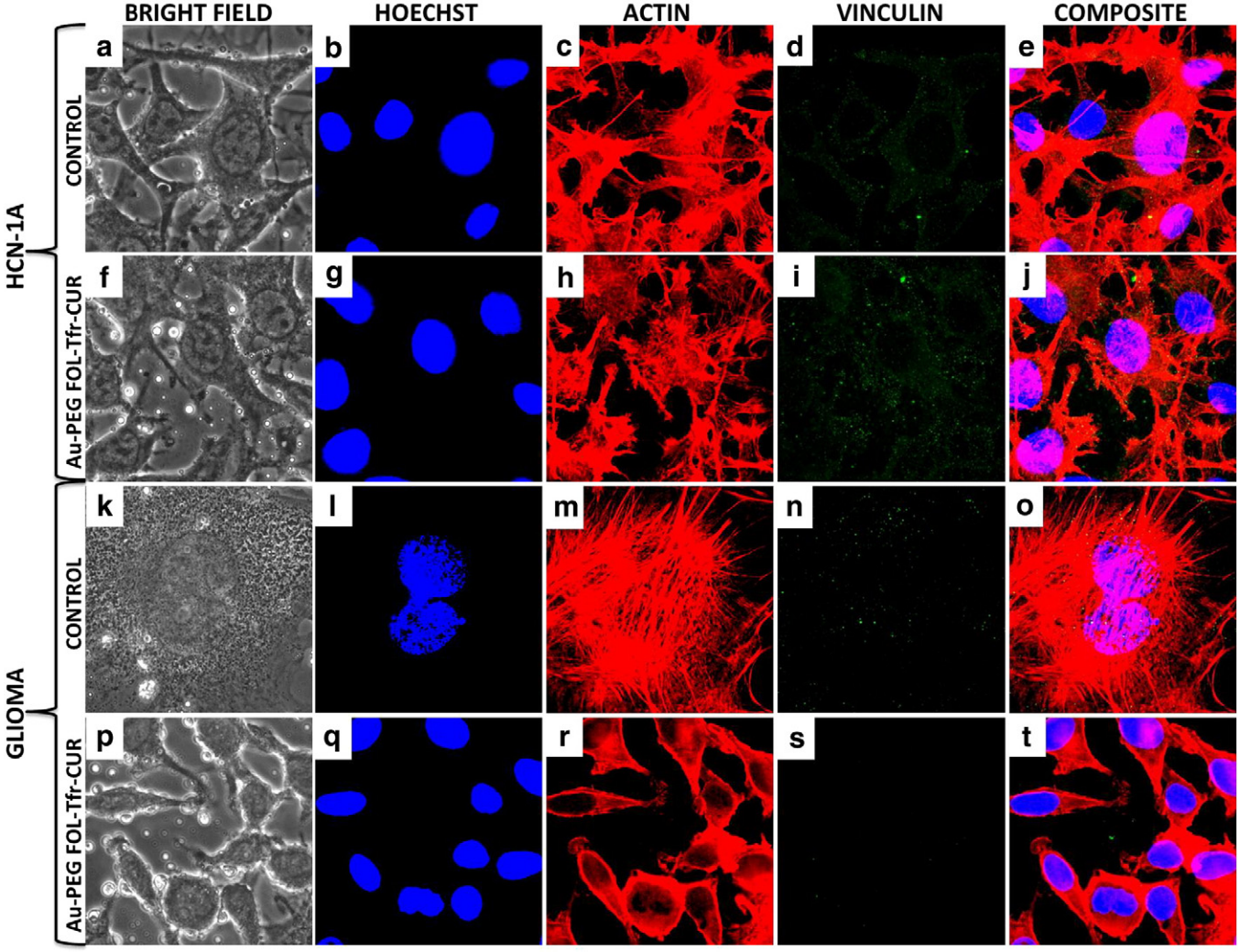

Fig. 7. Effect on vital cytoskeletal components. The complex organizational network of actin fibers (c, h and m), representative of a rigid and sturdy cytoskeletal architecture, was observed to be highly reduced and confined to circumferential regions in the Au-PEG-FOL-Tfr-CUR treated gliomas (r). A similar observation was recorded in the case of vinculin expression, which was significantly suppressed and feebly noticeable (s). The distortion and destabilization of these two essential structural proteins by the curcin conjugated Au NPs clearly demonstrates the proficiency of the nanoformulation in disabling the skeletal as well as cell–cell and cell–matrix assembly interaction .

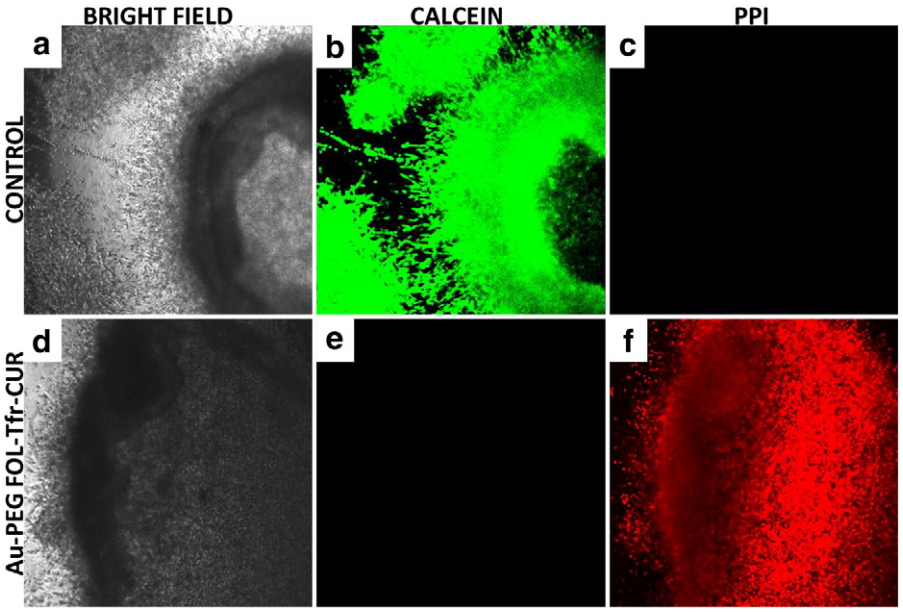

Fig. 8. Effect of curcin on 3D cancer colony. The control 3D colonies were 100% viable and positive to calcein (b). Prominent secondary colonies established around the parent mass were noted (a). The test colony (Au-PEG FOL-Tfr-CUR treated) appeared 100% positive to PPI (f) without the presence of any secondary colonies depicting the inability of cancer cells to proliferate, spread and metastasize under the influence of curcin. Also, the absence of any viable cells provides evidence for the deep penetration of the NPs to the interiors of the cancer mass, thereby effectuating greater levels of toxicity to the highly active and protected core.

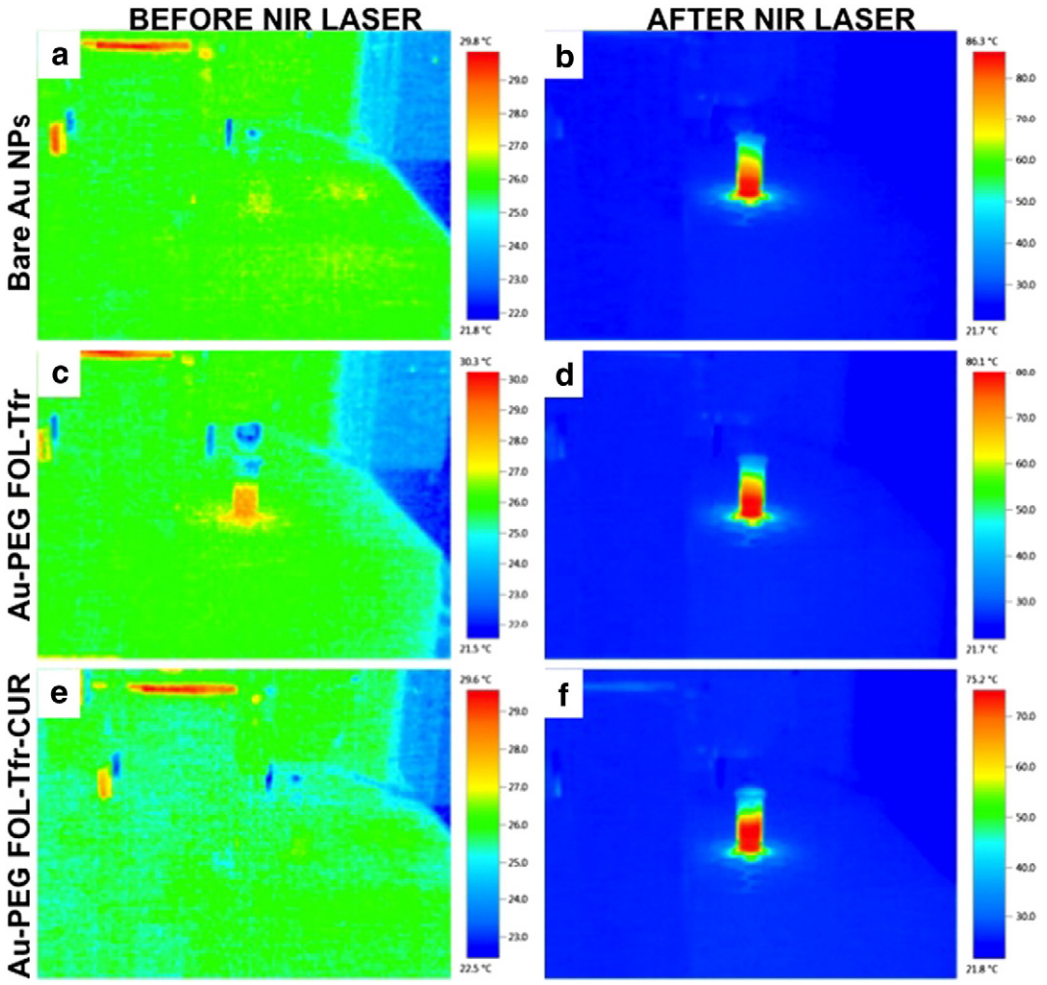

Fig. 9. NIR laser irradiation responsive temperature spikes in the Au nanoparticles were observed. The bare Au NPs, devoid of any surface functionalization exhibited a temperature rise of up to 86 °C (b). The functionalization of the NPs did not present any drastic effects on the thermal properties of the Au-PEG FOL-Tfr (d) or Au-PEG FOL-Tfr-CUR (f) with the former reaching a temperature high of 80 °C and the latter 75 °C.

FOL-Tfr treated HCN-1A and glioma (Fig. 4d, j) reinforces the superior cyto-compatibility of the nanoformulation. The ROS generation in the Au-PEG FOL-Tfr-CUR NP treated glioma cells, therefore, is the result of curcin which would have disrupted the mitochondrial potential, forcing the cells to trigger an ROS induced apoptotic pathway leading to their death, as observed in the cytotoxicity assay. To evaluate whether the elevated ROS levels have any secondary effects on cell physiology, mitochondrial membrane potential and DNA damage were evaluated.

Calcein based mitochondrial pore transition assay was carried out to analyze the effect of Au-PEG FOL-Tfr-CUR NPs on mitochondrial pore induction. It could be clearly observed that the control group (Fig. 5b, h) and Au-PEG FOL-Tfr-CUR NP treated HCN-1A cells (Fig. 5e) maintained discrete mitochondrial calcein staining. The co-localized green and red fluorescence confirmed the stability and rigidity of mitochondrial membrane with any pores. By contrast, Au-PEG FOL-Tfr-CUR NP treated glioma cells showed diminished if any calcein fluorescence (Fig. 5k), which depicted the leaching out of dye from the mitochondrial pores. In addition, loss of prominent fluorescence and patched signals in the cytosol evidenced the damage to mitochondrial membrane (Fig. 5l), induced as a result of direct effect of toxin exposure. On the basis of ROS production by cells when treated with curcin, it would be apt to relate the stress induced by the ROS to the loss of mitochondrial potential and subsequent disintegration. The uptake of mitotracker is dependent on the mitochondrion's activity, which is highly compromised during apoptosis. Mitochondrial dysfunction and loss of its membrane potential is known to trigger apoptotic signaling, leading to suicide of cells [33], which is the observed phenomenon in the Au-PEG FOL-Tfr-CUR NP treated glioma cells.

In terms of possible DNA damage, the occurrence of double-strand breaks was assessed by staining for γ-H2Ax foci, which are formed by the rapid phosphorylation of histone H2Ax at sites of DNA double-strand breaks [34]. The presence of double strand breaks, witnessed by the red dots in the nucleus, appeared in glioma cells (Fig. 6o) treated with Au-PEG FOL-Tfr-CUR NPs, whereas the control groups (Fig. 6c, k) and HCN-1A (Fig. 6g) showed any such incidence. Such a nuclear toxicity could be attributed to the direct entry of curcin into the nuclear region by disrupting the nuclear envelope leading to the DNA damage, as previous reports have suggested such a scenario with different RIPs [35,36] or due to the effects of forced entry of increased ROS in the nucleus.

Altogether, these observations focus on the severe secondary effects of elevated ROS levels when cells are exposed to Au-PEG FOL-Tfr-CUR NPs. As these results are in line with the onset of cytotoxic effects, the link between ROS induction and decreased cell viability was evident.

Apart from the stress on the mitochondria and nuclear regions, the effects of the same were assessed on the cytoskeletal framework composed of actin fibers. Control groups presented well-organized and elaborate actin network scaffolding throughout the cytoplasm (Fig. 7c,m) whereas glioma cells treated with Au-PEG FOL-Tfr-CUR NPs showed prominent actin filament degeneration and distortion with the fine fibrous network of actin reduced to circumferential linings and blurred hues (Fig. 7r). Generally, the cell begins to constrict as a

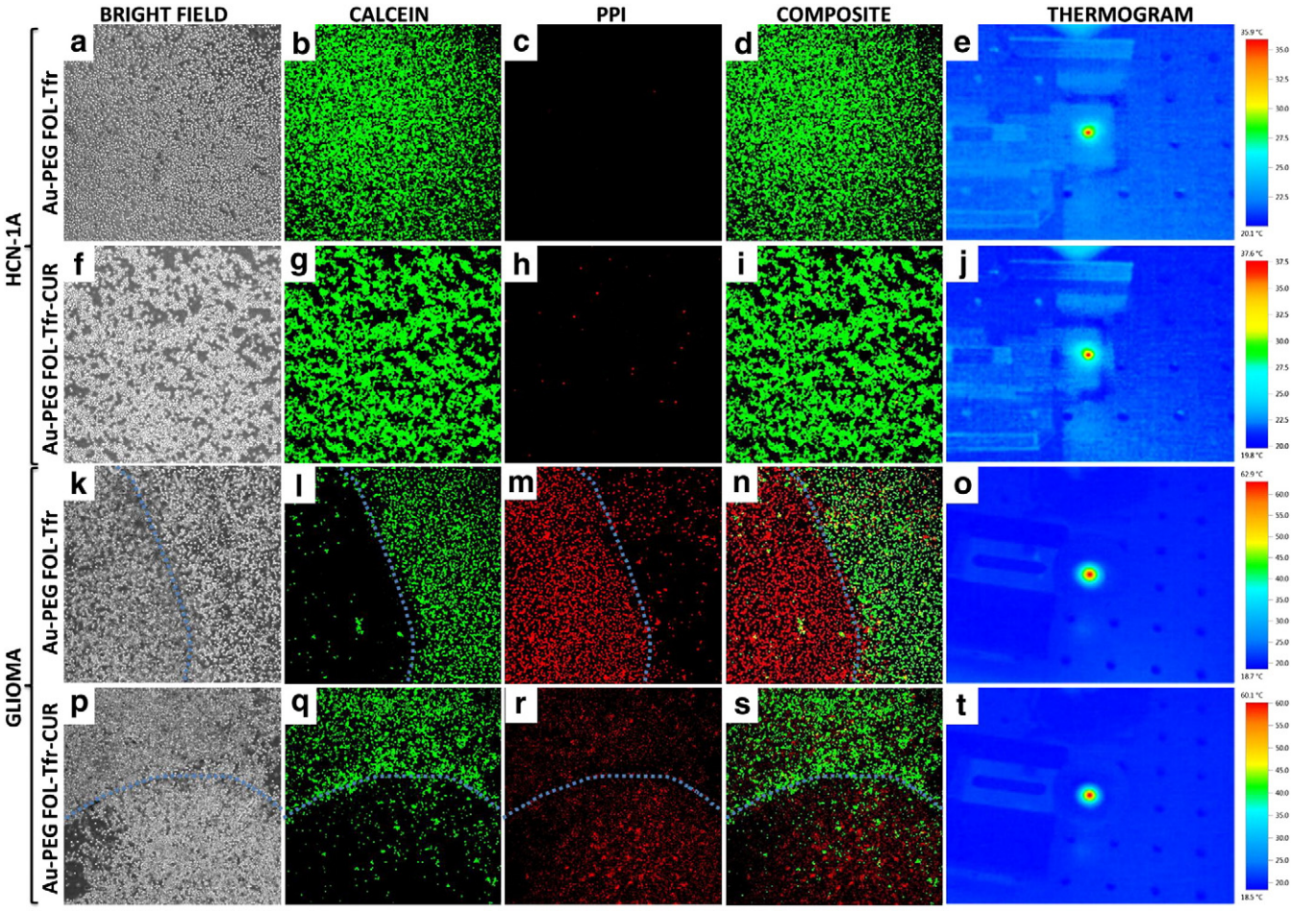

Fig. 10. NIR induced photothermal ablation of cancer cells utilizing Au-PEG FOL-Tfr and Au-PEG FOL-Tfr-CUR. Normal HCN-1A cells treated with Au-PEG FOL-Tfr and Au-PEG FOL-Tfr-CUR did not show rise in temperature above 36 °C (e) and 38 °C (j) respectively, and remained nearly 100% viable post NIR exposure (b, g). Glioma cells treated with Au-PEG FOL-Tfr showed a rapid rise in temperature reaching 63 °C (j) within 5 s. Approximately 90% of gliomas exhibited positive staining to PPI (m) within the zone of irradiation (dotted line) depicting necrotic cell death. Gliomas treated with Au-PEG FOL-Tfr-CUR, presented similar rise in temperature (t) and dead cell population as Au-PEG FOL-Tfr (r). The increased dead cells beyond the zone of irradiation in the case of Au-PEG FOL-Tfr-CUR is attributed to the curcin effect (r) symbolizing the synergistic action of photo-thermal and drug effects on cancer cells.

result of lamin and actin disruption in the cytoskeleton. After 48 h of Au-PEG FOL-Tfr-CUR NP treatment, cellular shrinkage leading to reduced total cellular volume was witnessed (Figs. 5j, 6m, 7p). In addition, highly reduced numbers of actin fibers with condensed staining patterns and the absence of tubular integrity were observed. Correlation to these irregularities in actin could be attributed to ROS signaling which was found to modify the integrity of actin and consequently the cell shape [37]. Also, extensive deformation of the actin fibers might have secondary effects on actin-mediated signaling pathways [38]. To investigate this possibility, the effect of the Au-PEG FOL-Tfr-CUR NPs on focal adhesion complexes (FACs) was assessed. FACs are composed of elaborate actin and vinculin networks, which create and maintain the structural integrity of the cell. Vinculin proteins are essential for cell–cell and cell–extra cellular matrix interactions. The proper expression of vinculin is vital for maintaining micro-environmental signal transductions. Curcin, the toxin used in the present study possesses ability to downregulate vinculin expression and architecture. The protein synthesis inhibitory activity of curcin [23,24] could be held responsible for such an effect. Emulating the same, Au-PEG FOL-Tfr-CUR NP treated glioma cells exhibited extremely diminished vinculin expression (Fig. 7s) which in conjunction with the loss of actin, reveals the high level of competence of such a nanoformulation in comprehensively disrupting the cytoskeletal organization of the target cells.

The culmination of various detrimental effects of the nanoformulation, encompassing mitochondrial, nuclear and structural dysfunction, strongly emphasize the exceptional proficiency of Au-PEG FOL-Tfr-CUR NPs against gliomas.

3.4. Drug effect of Au-PEG FOL-Tfr-CUR NPs on cancer 3D colonies

A profound reduction in the size of cancer mass, which led to shrinkage of 3D colony by 1/3 of its volume, was witnessed on treatment with the drug conjugated Au NPs. The live/dead analysis revealed a nearly 100% dead cell population (Fig. 8f). The control 3D mass, devoid of NP treatment, presented the formation of independent and interconnected small, secondary colonies with cellular protrusions indicative of migration and proliferation of the mass (Fig. 8a). These features were correlative of the aggressive infiltrative nature of gliomas under in vivo conditions. Such observations were completely absent in the Au-PEG FOL-Tfr-CUR NP treated group. There were no secondary colonies or the presence of any signs of migratory or proliferative attempts by the cancer mass, depicting the total arrest of cellular metabolism by curcin. A 3D in vitro colony mimics to an extent the nature of tumors in the in vivo system as the multi layers of cells portray the role of a barrier to curb the effects of drugs, NPs and related therapeutics by limiting them to the periphery of the tumors [39,40]. It is very rare that all the cells receive the intended dose of therapeutics as the cells shielded in the interior of the tumor mass are well protected from the desired toxic effects. The inability of major therapeutics to reach the core of tumors allows the recurrence of tumors over a period of time. The nano-formulation presented in this report successfully achieved complete dominance over the cancer mass, thereby nullifying the chances of further proliferation of the cancer cells.

3.5. Photothermal ablation of cancer cells

The excellent thermal competences of nanoconjugates on NIR laser irradiation (Fig. 9d, f) were efficiently utilized to impart selective ablation of the cancer cells. The prominent specificity of the Au NP conjugate has been reiterated in the observations so far. Within 5 s of laser irradiation the temperature of the glioma sample (Au-PEG FOL-Tfr) shot up to 60 ºC (Fig. 10o). A clear zone of irradiation demarcating the live (calcein stained) and dead (PPI stained) cells was witnessed (Fig. 10n). In the case of HCN-1A, the rise in temperature was significantly minimal with a final temperature of 35 ºC, which plateaued thereafter till 1 min of exposure (Fig. 10e) with the absence of any zones of irradiation. Similar results were recorded with the Au-PEG FOL-Tfr-CUR NP treated HCN-1A (Fig. 10h–j) with no significant rise in temperature. The glioma cells treated with Au-PEG FOL-Tfr-CUR NPs, presented added lethality by the dual action of photo-thermal and drug effects confirmed by the presence of increased numbers of dead cells outside the zone of laser irradiation (Fig. 10r). This particular observation could hold immense advantage in the case of in vivo solid tumors, where it is speculated that the released curcin may in fact enter the surrounding cancerous cells and invoke toxicity. This speculative claim can be correlated to the 3D spheroid destruction in Figs. 8 and

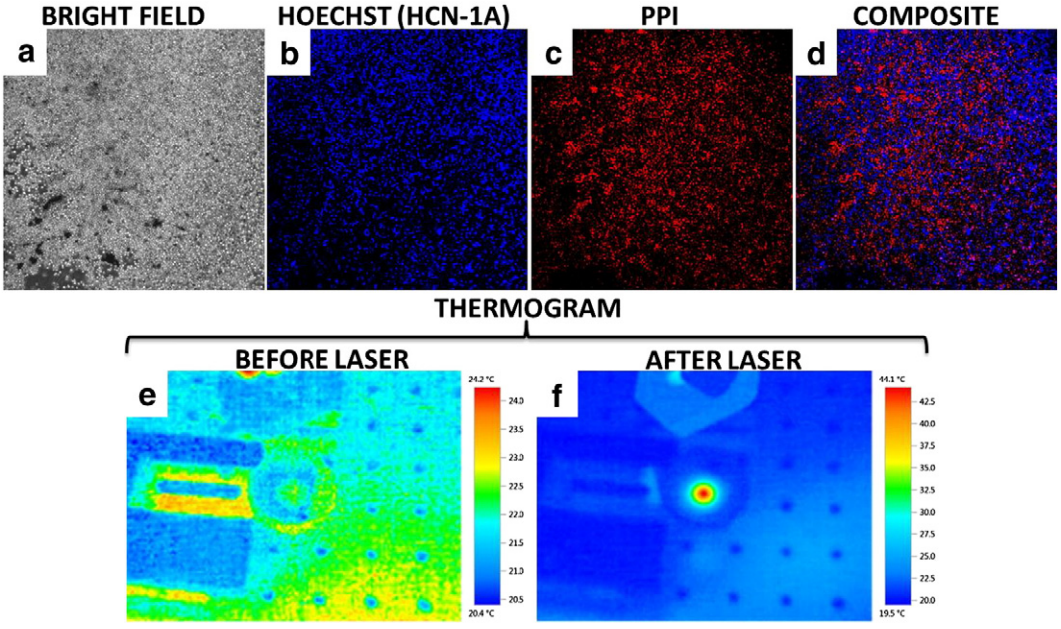

Fig. 11. NIR induced photothermal ablation with Au-PEG FOL-Tfr-CUR in co-culture. The normal HCN-1A cells were stained with nuclear marker Hoechst blue (b) to distinguish them from glioma (unstained). A rapid rise of temperature from 24 °C to 44 °C (e and f) was recorded within 5 s, during NIR exposure. Maximum of the normal cells remained viable as the co-localization of Hoechst and PPI staining in composite image was too few (d). Most of the PPI positive cells showed any blue fluorescence confirming their identity as gliomas. Nearly 95% of gliomas were dead whereas only less than around 10% of HCN-1A were positive to PPI.

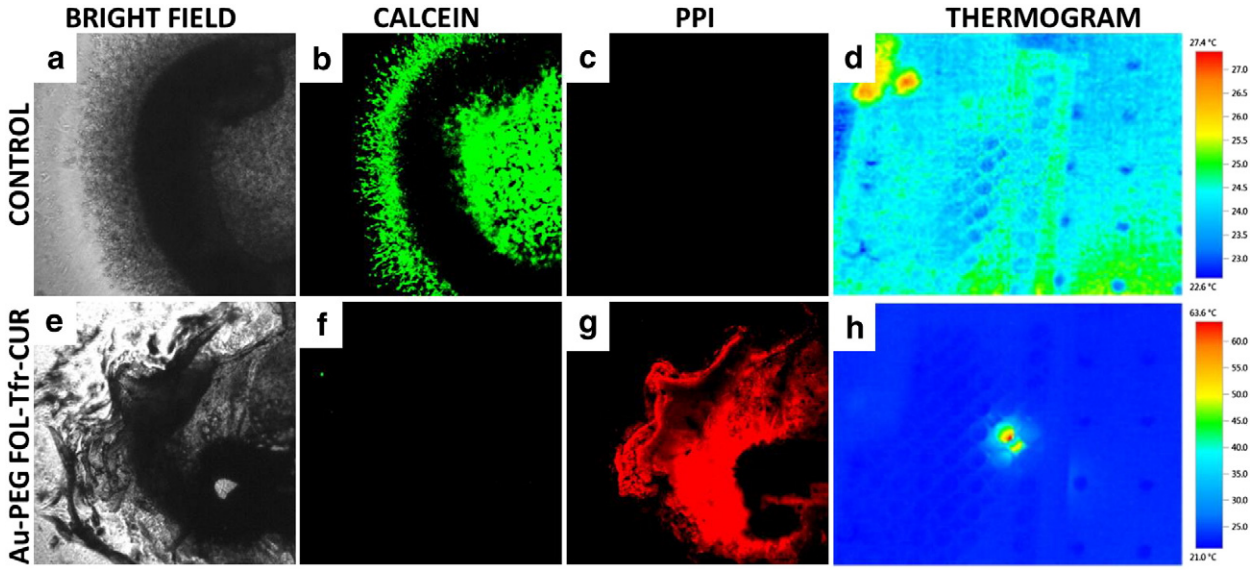

Fig. 12. Photo-thermal ablation of 3D glioma colonies using Au-PEG FOL-Tfr-CUR. The control colony (a) showed any rise in temperature (d) and displayed esterase activity of viable cells which were positive to calcein live cell marker (b) after NIR exposure. The Au-PEG FOL-Tfr-CUR treated colony was completely disrupted (e) by the sudden and detrimental rise in temperature (h) during NIR exposure. The morphology of 3D colony got completely disrupted and nearly all cells were positive to PPI (g) indicating the death of the cancer mass.

12, where the entire cancer mass was subject to extirpation. The selective ablation potency of the nanoformulation was tested on a glioma-HCN-1A co-culture (Fig. 11). HCN-1A cells were stained with Hoechst DNA marker to distinguish them from the unstained gliomas (Fig. 11b). The temperature sharply increased to 44 ºC within 5 s (Fig. 11f). The difference in temperature rise between the individual [60 ºC (Fig. 10t)] and co-cultures [44 ºC (Fig. 11f)] could be due to the lower number of Au nano-conjugates as a result of lower numbers of glioma cells in the co-culture experiments. Remarkably, the glioma population on laser irradiation was subject to near complete annihilation (stained with PPI) whereas the HCN-1A (blue) remained mostly viable (Fig. 11d). The viability of HCN-1A cells, post laser exposure in the co-culture experiments authenticates the supreme targeting efficiency attained with the Au-PEG FOL-Tfr-CUR NPs, thus providing another supportive stance for the utilization of such a nano-conjugate in future multi-modal therapeutic strategies.

The potential effects of the nano-conjugate on a 3D cancer mass were also tested. Upon NIR laser exposure, the temperature of the colony rose rapidly to 64 ºC within 5 s (Fig. 12h). The control colony, devoid of NPs, did not present any elevation in temperature for a period of 2 min, thus negating the role of geltrex in the temperature rise (Fig. 12d). Visual observation of ablated colonies under CLSM revealed a completely disrupted morphology (Fig. 12e). The live/dead staining presented a 100% dead cell population portraying the entire cancer mass as non-viable (Fig. 12g). The results, favor the nano-formulation's potential as a cogent candidate to effectively ablate solid tumors within a short period of time, completely and comprehensively eliminating them, leaving little scope for metastasis.

4. Conclusion

A multifunctional, folate and anti-transferrin antibody-conjugated, Au NP-based nanocarrier capable of delivering a potent anticancer drug, curcin specifically to brain cancer cells was developed for combined chemo- and photo-thermal therapy to gliomas. The cytocompatibility of the Au-PEG FOL-Tfr conjugates puts them in positive perspective in applications as drug delivery and the like. These Au NP-based nanocarriers exhibited high drug load capacity complemented with pH-sensitive drug release, which can minimize the nonspecific systemic spread of toxic drugs during circulation, while maximizing the efficiency of tumor-targeted anti-cancer drug delivery. The presence of dual tumor targeting ligands substantially increased the cellular uptake of the nano-conjugates by gliomas. Curcin as a model drug exhibited superior anti-proliferative and anti-migratory effects on cancer spheroids in addition to curbing the formation of secondary colonies with subsequent detrimental effects. In addition, the excellent photothermal ablation property of Au NPs, augmented with the advantage of cancer specific dual targeting were able to ablate cancer cells specifically in co-culture with normal cells as well as cancer spheroids effectively. The dual mode of lethality achieved with the photo-thermal ablation combined with effect of curcin proved extremely competent. Cumulatively, this nano-conjugate system is proposed as a paragon for future cancer treatment strategies to effectively and comprehensively restrict and destroy the cancer mass, negating the possibilities of future metastasis or recurrence.

Acknowledgements

M. Sheikh Mohamed would like to thank the Ministry of Education, Culture, Sports, Science and Technology (MEXT), Japan, for financially supporting this research. Part of this study has been supported by a grant for the program of strategic research foundation at private universities S1101017, organized by the Ministry of Education, Culture, Sports, Science and Technology (MEXT), Japan since April 2012. We thank the Japan Bio-Energy development Corporation (JBEDC), Japan, for generously providing the seeds of *J. curcas* for this study.

References

[1] R. Stupp, M.E. Hegi, Targeting brain-tumor stem cells, Nat. Biotechnol. 25 (2007) 193–194.
[2] M.F. Kircher, A.D. Zerda, J.V. Jokerst, C.L. Zavaleta, P.J. Kempen, E. Mittra, K. Pitter, R. Huang, C. Campos, F. Habte, R. Sinclair, C.M. Brennan, I.K. Mellinghoff, E.C. Holland, S.S. Gambhir, A brain tumor molecular imaging strategy using a new triple-modality MRI-photoacoustic-Raman nanoparticle, Nat. Med. 18 (2012) 829–834.
[3] S. Dhar, E.M. Reddy, A. Prabhune, V. Pokharkar, A. Shiras, B.L.V. Prasad, Cytotoxicity of sophorolipid-gellan gum-gold nanoparticle conjugates and their doxorubicin loaded derivatives towards human glioma and human glioma stem cell lines, Nanoscale 3 (2011) 575–580.
[4] Q. Hunag, Q.B. Zhang, J. Dong, Y.Y. Wu, Y.T. Shen, Y.D. Zhao, Y.D. Zhu, Y. Diao, A.D. Wang, Q. Lan, Glioma stem cells are more aggressive in recurrent tumors with malignant progression than in the primary tumor, and both can be maintained long-term in vitro, BMC Cancer 8 (2008) 304–313.
[5] J. Neman, R. Jandial, Decreasing glioma recurrence through adjuvant cancer stem cell inhibition, Biologics 4 (2010) 157–162.

[6] N.H. Sadraei, D.M. Peereboom, Chemotherapy in newly diagnosed primary central nervous system lymphoma, Ther. Adv. Med. Oncol. 2 (2010) 273–292.
[7] M.B. Søren, Preventing or reducing late side effects of radiation therapy: radiobiology meets molecular pathology, Nat. Rev. Cancer 6 (2006) 702–713.
[8] Y. Liu, H. Miyoshi, M. Nakamura, Nanomedicine for drug delivery and imaging: a promising avenue for cancer therapy and diagnosis using targeted functional nanoparticles, Int. J. Cancer 120 (2007) 2527–2537.
[9] S. Singh, Nanomedicine-nanoscale drugs and delivery systems, J. Nanosci. Nanotechnol. 10 (2010) 7906–7918.
[10] S.M. Moghimi, A.C. Hunter, J.C. Murray, Nanomedicine: current status and future prospects, FASEB J. 19 (2005) 311–330.
[11] M.S. Shim, Y. Kwon, Stimuli-responsive polymers and nanomaterials for gene delivery and imaging applications, Adv. Drug Deliv. Rev. 64 (2012) 1046–1059.
[12] S.R. Singh, H.E. Grossinklaus, S.J. Kang, H.F. Edelhauser, B.K. Ambati, U.B. Kompella, Intravenous transferrin, RGD peptide and dual-targeted nanoparticles enhance anti-VEGF intraceptor gene delivery to laser-induced CNV, Gene Ther. 16 (2009) 645–659.
[13] Q. Xu, Y. Liu, S. Su, W. Li, C. Chen, Y. Wu, Anti-tumor activity of paclitaxel through dual-targeting carrier of cyclic RGD and transferrin conjugated hyperbranched copolymer nanoparticles, Biomaterials 33 (2012) 1627–1639.
[14] D. Peer, J.M. Karp, S. Hong, O.C. Farokhzad, R. Margalit, R. Langer, Nanocarriers as an emerging platform for cancer therapy, Nat. Nanotechnol. 2 (2007) 751–760.
[15] M.C. Daniel, D. Astruc, Gold nanoparticles: assembly, supramolecular chemistry, quantum-size-related properties, and applications toward biology, catalysis, and nanotechnology, Chem. Rev. 104 (2004) 293–346.
[16] P. Ghosh, G. Han, M. De, C.K. Kim, V.M. Rotello, Gold nanoparticles in delivery applications, Adv. Drug Deliv. Rev. 60 (2008) 1307–1315.
[17] G. Han, P. Ghosh, V.M. Rotello, Functionalized gold nanoparticles for drug delivery, Nanomedicine 2 (2007) 113–123.
[18] V. Kattumuri, K. Katti, S. Bhaskaran, E.J. Boote, S.W. Casteel, G.M. Fent, D.J. Robertson, M. Chandrasekhar, R. Kannan, K.V. Katti, Gum arabic as a phytochemical construct for the stabilization of gold nanoparticles: *in vivo* pharmacokinetics and X-ray-contrast-imaging studies, Small 3 (2007) 333–341.
[19] G.M. Fent, S.W. Casteel, D.Y. Kim, R. Kannan, K. Katti, N. Chanda, K.V. Katti, Biodistribution of maltose and gum arabic hybrid gold nanoparticles after intravenous injection in juvenile swine, Nanomed. Nanotechnol. Biol. Med. 5 (2009) 128–135.
[20] J.D. Gibson, B.P. Khanal, E.R. Zubarev, Paclitaxel-functionalized gold nanoparticles, J. Am. Chem. Soc. 129 (2007) 11653–11661.
[21] W. Lu, C. Xiong, G. Zhang, Q. Huang, R. Zhang, J.Z. Zhang, C. Li, Targeted photothermal ablation of murine melanomas with melanocyte-stimulating hormone analog–conjugated hollow gold nanospheres, Clin. Cancer Res. 15 (2009) 876–886.
[22] R.C. Triulzi, Q. Dai, J. Zou, R.M. Leblanc, Q. Gu, J. Orbulescu, Q. Huo, Photothermal ablation of amyloid aggregates by gold nanoparticles, Colloids Surf. B: Biointerfaces 63 (2008) 200–208.
[23] L. Juan, Y. Fang, T. Lin, C. Fang, Antitumor effects of curcin from seeds of *Jatropha curcas*, Acta Pharmacol. Sin. 24 (2003) 241–246.
[24] M.J. Luo, X.Y. Yang, W.X. Liu, Y. Xu, P. Huang, F. Yan, F. Chen, Expression, purification and anti-tumor activity of curcin, Acta Biochim. Biophys. Sin. 38 (2006) 663–668.
[25] S.M. Mohamed, A. Baliyan, S. Veeranarayanan, A.C. Poulose, Y. Nagaoka, H. Minegishi, Y. Yoshida, T. Maekawa, D.S. Kumar, Non-destructive harvesting of biogenic gold nanoparticles from *Jatropha curcas* seed meal and shell extracts and their application as bio-diagnostic photothermal ablaters—lending shine to the biodiesel byproducts, NATE 1 (2012) 3–17.
[26] A.C. Poulose, S. Veeranarayanan, M.S. Mohamed, S. Raveendran, Y. Nagaoka, Y. Yoshida, T. Maekawa, D.S. Kumar, PEG coated biocompatible cadmium chalcogenide quantum dots for targeted imaging of cancer cells, J. Fluoresc. 22 (2012) 931–944.
[27] A.C. Poulose, S. Veeranarayanan, A. Aravind, Y. Nagaoka, Y. Yoshida, T. Maekawa, D.S. Kumar, Synthesis of $CuAlS_2$ nanocrystals and their application in bio-imaging, Mater. Express 2 (2012) 94–104.
[28] M.A. Dietrich, D. Zmijewski, H. Karol, A. Hejmej, B. Bilinska, P. Jurecka, I. Irnazarow, M. Slowinska, P. Hliwa, A. Ciereszko, Isolation and characterization of transferrin from common carp (*Cyprinus carpio* L.) seminal plasma, Fish Shellfish Immunol. 29 (2010) 66–74.
[29] W.C. Law, K.T. Yong, A. Baev, R. Hu, P.N. Prasad, Nanoparticle enhanced surface plasmon resonance biosensing: application of gold nanorods, Opt. Express 17 (2009) 19041–19046.
[30] Z. Yuan, Z. Que, S. Cheng, R. Zhuo, F. Li, pH-triggered blooming of 'nano-flowers' for tumor intracellular drug delivery, Chem. Commun. 48 (2012) 8129–8131.
[31] M. Hruby, C. Konak, K. Ulbrich, Polymeric micellar pH-sensitive drug delivery system for doxorubicin, J. Control. Release 103 (2005) 137–148.
[32] S. Veeranarayanan, A.C. Poulose, S.M. Mohamed, S.H. Varghese, Y. Nagaoka, Y. Yoshida, T. Maekawa, D.S. Kumar, Synergistic targeting of cancer and associated angiogenesis using triple-targeted dual-drug silica nanoformulations for theragnostics, Small 8 (2012) 3476–3489.
[33] M. Crompton, The mitochondrial permeability transition pore and its role in cell death, Biochem. J. 341 (1999) 233–249.
[34] S.J. Soenen, B. Manshian, J.M. Montenegro, F. Amin, B. Meermann, T. Thiron, M. Cornelissen, F. Vanhaecke, S. Doak, W.J. Parak, Cytotoxic effects of gold nanoparticles: a multiparametric study, ACS Nano 6 (2012) 5767–5783.
[35] E.A. Hassoun, X. Wang, Time- and concentration-dependent production of superoxide anion, nitric oxide, DNA damage and cellular death by ricin in the J774A.1 macrophage cells, J. Biochem. Mol. Toxicol. 13 (1999) 179–185.
[36] M. Brigotti, R. Alfieri, P. Sestili, M. Bonelli, P.G. Petronini, A. Guidarelli, L. Barbieri, F. Stirpe, S. Sperti, Damage to nuclear DNA induced by Shiga toxin 1 and ricin in human endothelial cells, FASEB J. 16 (2002) 365–372.
[37] H. Lum, K.A. Roebuck, Oxidant stress and endothelial cell dysfunction, Am. J. Physiol. Cell Physiol. 280 (2001) C719–C741.
[38] S.J. Soenen, N. Nuytten, S.F. De Meyer, S.C. De Smedt, M. De Cuyper, High intracellular iron oxide nanoparticle concentrations affect cellular cytoskeleton and focal adhesion kinase-mediated signaling, Small 6 (2010) 832–842.
[39] N. Linde, C.M. Gutschalk, C. Hoffmann, D. Yilmaz, M.M. Mueller, Integrating macrophages into organotypic co-cultures: a 3D in vitro model to study tumor-associated macrophages, Plos One 7 (2012) e40058.
[40] E. Krausz, R. Hoogt, E. Gustin, F. Cornelissen, T. Grand-Perret, L. Jannsen, N. Vloemans, Translation of a tumor microenvironment mimicking 3D tumor growth co-culture assay platform to high-content screening, J. Biomol. Screen. 18 (2013) 54–66.